

BROADBAND X-RAY SPECTRA OF GX 339–4 AND THE GEOMETRY OF ACCRETING BLACK HOLES IN THE HARD STATE

JOHN A. TOMSICK¹, EMRAH KALEMCI², PHILIP KAARET³, SERA MARKOFF⁴, STEPHANE CORBEL⁵, SIMONE MIGLIARI⁶, ROB FENDER⁷, CHARLES D. BAILYN⁸, MICHELLE M. BUXTON⁸

Accepted by the Astrophysical Journal

ABSTRACT

A major question in the study of black hole binaries involves our understanding of the accretion geometry when the sources are in the “hard” state. In this state, the X-ray energy spectrum is dominated by a hard power-law component and radio observations indicate the presence of a steady and powerful “compact” jet. Although the common hard state picture is that the accretion disk is truncated, perhaps at hundreds of gravitational radii (R_g) from the black hole, recent results for the recurrent transient GX 339–4 by Miller and co-workers show evidence for optically thick material very close to the black hole’s innermost stable circular orbit. That work focused on an observation of GX 339–4 at a luminosity of about 5% of the Eddington limit (L_{Edd}) and used parameters from a relativistic reflection model and the presence of a soft, thermal component as diagnostics. In this work, we use similar diagnostics, but extend the study to lower luminosities (2.3% and 0.8% L_{Edd}) using *Swift* and *RXTE* observations of GX 339–4. We detect a thermal component with an inner disk temperature of ~ 0.2 keV at 2.3% L_{Edd} . At 0.8% L_{Edd} , the spectrum is consistent with the presence of such a component, but the component is not required with high confidence. At both luminosities, we detect broad features due to iron $K\alpha$ that are likely related to reflection of hard X-rays off the optically thick material. If these features are broadened by relativistic effects, they indicate that optically thick material resides within $10 R_g$ down to 0.8% L_{Edd} , and the measurements are consistent with the inner radius of the disk remaining at $\sim 4 R_g$ down to this level. However, we also discuss an alternative model for the broadening, and we note that the evolution of the thermal component is not entirely consistent with the constant inner radius interpretation. Finally, we discuss the results in terms of recent theoretical work by Liu and co-workers on the possibility that material may condense out of an Advection-Dominated Accretion Flow to maintain an inner optically thick disk.

Subject headings: accretion, accretion disks — black hole physics — stars: individual (GX 339–4) — X-rays: stars — X-rays: general

1. INTRODUCTION

Over the past several years, progress has been made in constraining the geometry of black hole accretion disks. Most binaries with stellar mass black holes are X-ray transients, and X-ray observations made when the sources are bright ($L_x \sim 10^{37-39}$ ergs s^{−1}) have uncovered iron $K\alpha$ emission lines with broad and redshifted profiles thought to be produced via fluorescence when hard X-rays reflect off optically thick disk material (Reynolds & Nowak 2003). Fitting the energy spectra with relativistic reflection models yield inner disk radii close to the innermost stable circular orbit (ISCO) of the black hole (Miller et al. 2002). Another constraint comes from the high frequency (100–500 Hz) quasi-periodic oscillations (QPOs) that are present for a number of black hole systems (Remillard et al. 2002). Although the origin of these QPOs is

still unclear, if they are related to Keplerian orbital frequencies for matter in an optically thick (e.g., Shakura & Sunyaev 1973) accretion disk, they correspond to time scales very close to the ISCO, implying that the disk must extend near the black hole. Furthermore, these constraints on the inner radius of the accretion disk (R_{in}) occurred at times when the X-ray energy spectrum included a strong thermal component that is consistent with the Shakura & Sunyaev (1973) model with an inner disk temperature of ~ 1 keV and an inner radius close to or at the ISCO.

As black hole outbursts evolve, they enter different spectral states, and one definition for the various states was recently described in McClintock & Remillard (2006). While the iron lines, QPOs, and thermal components discussed above have provided a determination of R_{in} in the “thermal-dominant” and “steep power-law” (SPL) spectral states, in this work, we focus on the hard state where the accretion disk geometry is still unclear. The hard state is most often observed at the beginning and end of the outburst and is characterized by a hard energy spectrum and a high level of X-ray timing noise. At the ends of outbursts, the hard state is most often seen when sources reach Eddington-scaled luminosities below $L/L_{\text{Edd}} = 0.01\text{--}0.04$ (Maccarone 2003), but the hard state also can occur at higher luminosities, especially when outbursts commence. Radio observations have made it clear that a steady outflow in the form of a “compact” jet is characteristic of the hard state (Fender 2001), and, at least in some systems, the jet power is inferred to be more than 20% of the X-ray luminosity (Fender et al. 2001). Thus, one reason that it

¹ Space Sciences Laboratory, 7 Gauss Way, University of California, Berkeley, CA 94720-7450, USA (e-mail: jtomsick@ssl.berkeley.edu)

² Sabanci University, Orhanli - Tuzla, Istanbul, 34956, Turkey

³ Department of Physics and Astronomy, University of Iowa, Van Allen Hall, Iowa City, IA 52242, USA.

⁴ Astronomical Institute ‘Anton Pannekoek’, University of Amsterdam, Kruislaan 403, 1098 SJ, Amsterdam, The Netherlands.

⁵ AIM - Unité Mixte de Recherche CEA - CNRS - Université Paris VII - UMR 7158, CEA-Saclay, Service d’Astrophysique, 91191 Gif-sur-Yvette Cedex, France.

⁶ Center for Astrophysics and Space Sciences, University of California San Diego, 9500 Gilman Dr., La Jolla, CA 92093-0424, USA.

⁷ School of Physics and Astronomy, University of Southampton, Hampshire SO17 1BJ, United Kingdom.

⁸ Department of Astronomy, Yale University, P.O. Box 208101, New Haven, CT 06520, USA.

is important to understand the disk geometry and other physical processes that occur in the hard state is that this is the one state that is linked to the production of a steady and powerful jet.

The common picture for the hard state accretion disk has been that its inner edge recedes (i.e., R_{in} increases), leaving a hot flow, such as an Advection-Dominated Accretion Flow (ADAF) or a spherical corona, where most of the X-ray emission is produced via Comptonization (Narayan, McClintock & Yi 1996; Esin, McClintock & Narayan 1997). Indeed, it has been shown that evaporation of the accretion disk can lead to a truncated disk at low mass accretion rates (Meyer, Liu & Meyer-Hofmeister 2000). From an observational standpoint, several measurements are suggestive of a truncated disk, but no one method provides a direct measurement of R_{in} . Examples of measurements that support an increase in R_{in} include a rapid drop in the temperature and flux of the thermal component (often to non-detection in the >3 keV band) as the source enters the hard state as well as a drop in the characteristic frequencies seen in the power spectra (Poutanen, Krolik & Ryde 1997; Dove et al. 1997; Tomsick & Kaaret 2000; Revnivtsev, Gilfanov & Churazov 2001; Kalemci et al. 2004; Tomsick, Kalemci & Kaaret 2004). In addition, a gradual drop in the strength of the reflection component can be explained if the disk is truncated and there is overlap between the disk and corona (Zdziarski, Lubinski & Smith 1999; Zdziarski et al. 2003).

While these measurements can be explained within the truncated disk picture, other explanations have also been suggested. Much of the evidence for the disappearance of the thermal component come from *RXTE* spectra that lack soft X-ray coverage, allowing for the possibility that the thermal component simply shifts out of the instrumental bandpass. Also, an increase in the ionization state of the inner disk could cause a drop in the strength of the reflection component. In addition, some recent X-ray observations of black holes in their hard state cast doubt on whether the truncated disk picture is correct. The black hole system GX 339–4 was observed in the hard state with *XMM-Newton* and the *Rossi X-ray Timing Explorer (RXTE)*, and a fit with reflection and iron line emission components accounting for relativistic smearing effects are consistent with an inner disk radius very close to the ISCO (Miller et al. 2006). The ISCO is at $6R_g$ (where $R_g = GM/c^2$, G and c are constants, and M is the black hole mass) for a non-rotating black hole and at $1.23R_g$ for a black hole rotating at the limiting spin rate of $a_* = 0.9982$ (Thorne 1974), where a_* is the mass-normalized angular momentum parameter. Miller et al. (2006) obtained a value of $R_{\text{in}}/R_g = 4.0 \pm 0.5$ from the GX 339–4 hard state X-ray spectra. As this value is only slightly larger than the value of $2\text{--}3 R_g$ that Miller et al. (2004) obtained for GX 339–4 in the SPL state, it suggests that there is very little change in R_{in} between the two states. However, we must keep in mind that the interpretation of the relativistic smearing parameters depend on the model being physically correct, and other explanations have been advanced for iron line broadening (e.g., Laurent & Titarchuk 2007).

For the thermal component from an optically thick disk, one expects the emission to fall outside the X-ray regime if R_{in} increases dramatically (e.g., to hundreds of R_g or more) as predicted by ADAF models (McClintock et al. 2003). However, there are numerous examples of black hole systems, includ-

ing well-known systems such as Cygnus X-1 and GX 339–4, that exhibit thermal X-ray emission with temperatures 0.1–0.4 keV when they are in the hard state (Ebisawa et al. 1996; Zdziarski et al. 1998). While this implies that very large values of R_{in} are not required for black holes to enter the hard state, the thermal components have been found mostly only when the systems are in the brightest phases of their hard states. For example, the *XMM-Newton/RXTE* observation of GX 339–4 in the hard state described above occurred at the start of an outburst at $L/L_{\text{Edd}} = 0.05$ and spectral fits yielded a thermal component with a temperature of ~ 0.4 keV. X-ray observations of other black hole systems at lower X-ray luminosities have provided relatively high quality X-ray spectra, and, in some cases, soft components have been detected (e.g., Miller, Homan & Miniutti 2006), while, in other cases, they have not (e.g., McClintock et al. 2001; Tomsick, Kalemci & Kaaret 2004).

For this paper, we have obtained broadband *Swift* (Gehrels et al. 2004) and *RXTE* (Bradt, Rothschild & Swank 1993) observations of the recurrent transient GX 339–4 in the hard state to constrain the accretion disk geometry in this state. The observations were made at the end of the most recent outburst that began in 2007 January (Miller et al. 2007) after the transition to the hard state that occurred in 2007 May (Kalemci et al. 2007). The luminosities of the observations we use in this work are well below $L/L_{\text{Edd}} = 0.05$, and our goal is to use the spectra along with reflection models that account for relativistic effects to constrain the accretion geometry at these low luminosities.

2. OBSERVATIONS

2.1. *RXTE* Monitoring Observations

We obtained daily pointed *RXTE* monitoring observations of GX 339–4 starting on 2007 April 20 (MJD 54,210) when the flux dropped below 4×10^{-9} ergs cm $^{-2}$ s $^{-1}$ as measured in the 1.5–12 keV band by the *RXTE* All-Sky Monitor. Observations were made under our program (proposal #92704) until 2007 July 18 (MJD 54,299), and the *RXTE* Proportional Counter Array (PCA Jahoda et al. 2006) 3–25 keV light curve during this 89 day period is shown in Figure 1. The exposure times were typically 1–3 ks for these monitoring observations although some longer *RXTE* observations were also obtained as described below. We reported an increase in timing noise and a hardening of the GX 339–4 energy spectrum that indicates a change to the hard-intermediate state (see Homan & Belloni 2005) occurred on 2007 May 12 (Kalemci et al. 2007), and this is marked in Figure 1 with a vertical dotted line at MJD 54,232. By 2007 May 22 (marked in Figure 1 by the vertical dashed line at MJD 54,242), the source had reached the hard state with an energy spectrum dominated by a power-law with a photon index of $\Gamma = 1.6$. Further evidence that the source reached the hard state by this time includes an increase in the optical and infrared flux (Buxton & Bailyn 2007) as well as core radio flux (S. Corbel, private communication), which is an indication for the presence of a compact jet.

2.2. *Swift* and *RXTE* Observations

The main focus of this work is the study of the broadband $\sim 1\text{--}200$ keV energy spectra from GX 339–4 at two times after the source made a transition to the hard state. As indicated in Figure 1, the first *Swift* observation occurred on 2007 May 25 (MJD 54,245), a few days after the transition to the hard state.

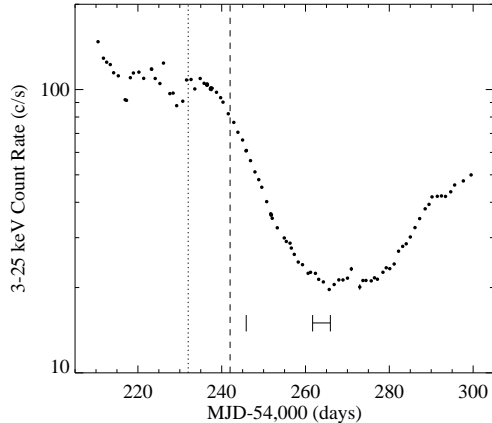


FIG. 1.— The 3–25 keV light curve for GX 339–4 as measured by the *RXTE*/PCA. The rates shown are for a single Proportional Counter Unit (PCU2). The vertical dotted line shows the start of the transition to the hard state, and the vertical dashed line shows when the source reached the hard state. The times of the *Swift* observations at MJD 54,245 and MJD 54,261–54,265 are marked.

The average *Swift* X-ray Telescope (XRT Burrows et al. 2005) count rate during the 6150 s observation was 10.41 ± 0.04 c s⁻¹ (0.8–8 keV). As indicated in Table 1, we obtained *RXTE* observations that were simultaneous with much of the *Swift* observation. The average PCA count rate was 44.1 ± 0.1 c s⁻¹ (3.6–25 keV) for Proportional Counter Unit (PCU) #2, and the average High Energy X-ray Timing Experiment (HEXTE Rothschild et al. 1998) count rate was 10.4 ± 0.2 c s⁻¹ (17–240 keV) for HEXTE cluster B. As described below, Spectrum #1 consists of the spectra from XRT, PCA, and HEXTE from these observations.

We used the same 3 instruments for Spectrum #2, but the observations were made 2–3 weeks later during the time period 2007 June 10–14. Table 1 shows that there were 3 *Swift* and 5 *RXTE* observations made during this time frame. Although the *Swift* and *RXTE* observations were mostly not strictly simultaneous, the source did not show large changes in count rate or spectral hardness over the 5 day period. The 3.6–25 keV PCA count rates for each of the 5 observations listed in Table 1 were 16.4 ± 0.1 c s⁻¹, 16.2 ± 0.1 c s⁻¹, 15.7 ± 0.2 c s⁻¹, 15.1 ± 0.1 c s⁻¹, and 14.2 ± 0.1 c s⁻¹, showing a gradual but not dramatic decline. As shown in Figure 1, this period is close to the minimum flux that GX 339–4 obtained before its flux began increasing again. The average *Swift* XRT count rate was 2.86 ± 0.02 c s⁻¹ (0.8–8 keV), while the average PCU2 and HEXTE-B count rates were 15.6 ± 0.1 c s⁻¹ (3.6–25 keV) and 3.8 ± 0.2 c s⁻¹ (17–240 keV), respectively. Thus, when compared to Spectrum #1, the XRT count rate is lower by a factor of 3.6 while the count rates for the *RXTE* instruments are lower by a factor of ~ 2.8 .

3. SPECTRAL ANALYSIS

We performed spectral analysis using XRT, PCA, and HEXTE data from the observations described above. To extract the spectra, we used the *Swift* and *RXTE* tools provided in the HEASOFT v6.3.1 software package. The XRT instrument consists of a CCD imager at the focus of a grazing incidence X-ray telescope. Although the instrument is capable of two-dimensional imaging for faint sources, our target was bright enough to require the use of Windowed Timing mode, which provides one-dimensional imaging. For the GX 339–

4 energy spectra, we determined the one-dimensional centroid of the target and extracted the photons within 47'' of the centroid. We also extracted background spectra that include photons from regions between 77'' and 171'' from the GX 339–4 centroid. We used version 9 of the XRT response matrix and kept events with grades in the range 0–2 (swxwt0_20010101v009.rmf). In addition, we produced an ancillary response file (ARF) with the HEASOFT tool *xrtmkarf* v0.5.3. In making the ARF file, we used an exposure map produced with the tool *xrtexpomap* v0.2.2.

For the PCA spectra, we used the SkyVLE background model that was most recently updated 2005 November 28⁹, and we used the HEASOFT tool *pcarsp* v10.1 to produce the response matrix. Although the PCA has 5 PCUs, it is typical that only 2 or 3 PCUs will be turned on for a given observation. In our case, only PCUs 0 and 2 were turned on for all of our *RXTE* observations. Due to the loss of the PCU 0 propane layer, this PCU's response is not as well known as the other PCUs (Jahoda et al. 2006). Also, for all the PCUs, the response for the top anode layer (where most of the counts are detected) is better modeled than the bottom layers. Thus, for this study, we only used the top anode layer of PCU 2 when extracting spectra. To check on the level of systematic error, we extracted the PCU 2 spectrum for the Crab nebula using Observation ID 92802-01-22-00, which is an observation from 2007 May 14. Fitting the spectrum with an absorbed power-law, we find that 1% systematic errors are required to reach a reduced- χ^2 near 1.0, and we use 1% systematics for the GX 339–4 spectra as well. For the HEXTE spectra, we used only HEXTE-B because HEXTE-A no longer obtains background measurements.

We performed preliminary spectral fits to Spectrum #1 to check on the agreement between the calibrations of the different instruments. For these preliminary fits, we used XRT, PCA, and HEXTE data in the 0.3–10 keV, 2.75–25 keV, and 17–240 keV energy bands, respectively. We used XSPEC v12 and fitted the spectra with an absorbed power-law model. We also included a multiplicative constant in the model to allow for differences in the overall normalizations between instruments. The fact that we obtain a poor fit ($\chi^2/\nu = 1282/269$) is partially due to the fact that the power-law model is too simple as well as being due to instrument calibrations. For example, it is known that the XRT calibration is complicated by features due to the SiO₂ layer in the CCD detectors at low energies (Osborne et al. 2005). In fact, we see a sharp dip in the XRT residuals near 0.5–0.6 keV that is likely instrumental. Furthermore, we see that the XRT calibration does not agree with the PCA calibration above 8 keV, and these issues lead us to use the XRT in the 0.8–8 keV energy range for the fits described below. In addition, the PCA calibration does not agree with XRT at the very bottom of the PCA range as there are strong positive residuals in the PCA spectrum below 3.6 keV. Thus, in the following, we use the 3.6–25 keV PCA spectrum. PCA and HEXTE match well in the region where they overlap, and we use the full 17–240 keV HEXTE bandpass. In addition, we note that there is good agreement (within 5%) between the overall normalizations of the three instruments.

⁹ A problem with the software that produces PCA background spectra was recently announced (see http://heasarc.gsfc.nasa.gov/docs/xte/xte_1st.html). We re-extracted the spectra with the corrected software and found that the problem did not impact our observations.

For PCA, Spectra #1 and #2 have high statistical quality (hundreds or thousands of counts per energy bin) across the bandpass, but some rebinning was required for XRT and HEXTE. For XRT, we rebinned from 719 channels to 148 channels, leaving averages of 432 counts/bin and 259 counts/bin for Spectra #1 and #2, respectively. We rebinned the HEXTE spectra from 210 channels to 22 channels.

4. RESULTS

4.1. Fits with Basic Models: Is a Thermal Disk Component Present?

We fitted the spectra with an absorbed power-law model. To account for absorption, we use the photoelectric absorption cross sections from Balucinska-Church & McCammon (1992) and elemental abundances from Wilms, Allen & McCray (2000), which correspond to the estimated abundances for the interstellar medium. A power-law model does not provide a good fit to either spectrum, with χ^2 equal to 651.8 and 321.6 for Spectra #1 and #2, respectively (for 213 degrees of freedom in both cases). Figures 2 and 3 show the spectra and the residuals in the form of a data-to-model ratio. In both cases, the strongest feature in the residuals occurs in the region near the iron $K\alpha$ region. Positive residuals are present close to the $\sim 6\text{--}7$ keV range where an emission line might be expected to be present, and negative residuals are seen from 7 keV to beyond 10 keV. The positive residuals that are present in the 20–40 keV range, especially in Spectrum #1, may be due to a reflection component. Finally, the curvature in the residuals at the lower end of Spectrum #1 may indicate the presence of a thermal component from an optically thick accretion disk. The fit parameters are given in Table 2, and it is notable that column density of $N_{\text{H}} = (3.1 \pm 0.1) \times 10^{21} \text{ cm}^{-2}$ obtained for the power-law fit to Spectrum #1 is somewhat lower than the value inferred from the work of Hynes et al. (2004). From optical observations, Hynes et al. (2004) prefer a value of $E(B-V) \gtrsim 0.85$, which corresponds to $N_{\text{H}} \gtrsim 4.7 \times 10^{21} \text{ cm}^{-2}$ using conversions given in Predehl & Schmitt (1995). Thus, the lower column density could also be an indication that a thermal component is present.

To test whether a thermal component is present in the spectra, we performed the fits detailed in Table 2. For Spectrum #1, when we add a disk-blackbody (Mitsuda et al. 1984) component to the power-law, the quality of the fit shows a large improvement to $\chi^2/\nu = 532.0/211$. This, in addition to the fact that the N_{H} increases to a level which is consistent with the lower limit from optical extinction measurements, are indications for the presence of a thermal component. However, even with the disk-blackbody component, the fit is poor due to the iron features in the spectrum, so we re-fitted Spectrum #1 with a model that takes these features into account. Although we use a more physical model for the iron line and reflection below, here we add a smeared iron edge (Ebisawa et al. 1994) to the model because it is a simple addition that significantly improves the fit. When the disk-blackbody component is added to a model with a power-law and a smeared edge, the fit shows a large improvement from $\chi^2/\nu = 444.7/211$ to 338.3/209.

We carried out the same series of fits for Spectrum #2, and while they also provide evidence for the presence of a thermal component, the evidence is considerably weaker than for Spectrum #1. For the models without the smeared edge (see Table 2), adding the disk-blackbody component gives a rela-

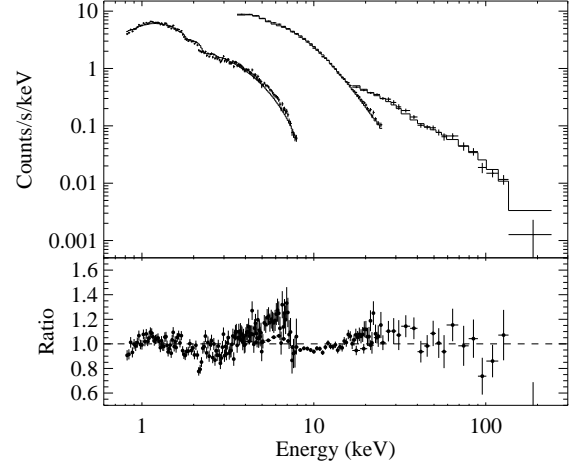


FIG. 2.— Spectrum #1, including data from *Swift*/XRT (0.8–8 keV), *RXTE*/PCA (3.6–25 keV), and *RXTE*/HEXTE (17–240 keV), fitted with an absorbed power-law model. The data-to-model ratio is shown in the bottom panel.

tively large improvement in the fit from $\chi^2/\nu = 321.6/213$ to 280.1/211. However, with the smeared edge, the change from $\chi^2/\nu = 210.6/211$ to 200.2/209 is rather small.

To further test the significance of the thermal component in the spectra and to determine if there is any evolution in the thermal component between Spectra #1 and #2, we produced error contours for the disk-blackbody temperature (kT_{in}) and normalization (N_{DBB}). In Figure 4, the outermost contour for each spectrum corresponds to 90% confidence for two-parameters of interest ($\Delta\chi^2 = 4.61$). The error region for Spectrum #1 shows that N_{DBB} is significantly different from zero, consistent with the presence of a thermal component in Spectrum #1. The error region for Spectrum #2 is well-separated from that of Spectrum #1, showing a clear change in the thermal component between the two spectra. The results indicate a drop in kT_{in} or N_{DBB} or both parameters. To estimate the significance of the thermal component in Spectrum #2, we adjusted $\Delta\chi^2$ until the confidence contour reached a N_{DBB} value of zero. The 99% confidence contour ($\Delta\chi^2 = 9.21$) does not reach zero, but zero is reached with a slightly larger contour ($\Delta\chi^2 = 10$), which is consistent with a $\sim 1\%$ chance that this component is spurious.

4.2. Iron Line and Reflection Modeling

We re-fitted the spectra in an attempt to improve our modeling of the iron line and reflection. Initially, we removed the smeared edge and fitted the spectra with a model consisting of a disk-blackbody, a power-law, and a Gaussian emission line. Although the Gaussian greatly improves the fit in both cases, the energy is well below the 6.4–7.1 keV iron range with values of $E_{\text{line}} = 3.8^{+0.6}_{-0.8}$ keV and $4.0^{+0.8}_{-1.4}$ keV for Spectra #1 and #2, respectively. As suggested by the residuals in Figures 2 and 3, the Gaussians are also very broad with widths of $\sigma \sim 2.0$ keV in both cases. This suggests that we may be seeing relativistically smeared iron lines.

The *laor* emission line model (Laor 1991) is appropriate for reflection from an accretion disk around a rotating black hole, and if the iron line is due to reflection, then one expects to see evidence for excess emission from reflection at higher energies ($\sim 20\text{--}40$ keV) as well. In fact, the positive residuals for Spectrum #1 (and to some extent for Spectrum #2) in this

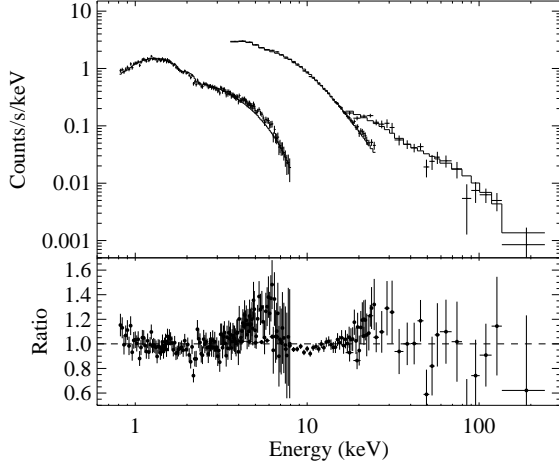


FIG. 3.— Spectrum #2, including data from the XRT, PCA, and HEXTE instruments, fitted with an absorbed power-law model. The data-to-model ratio is shown in the bottom panel.

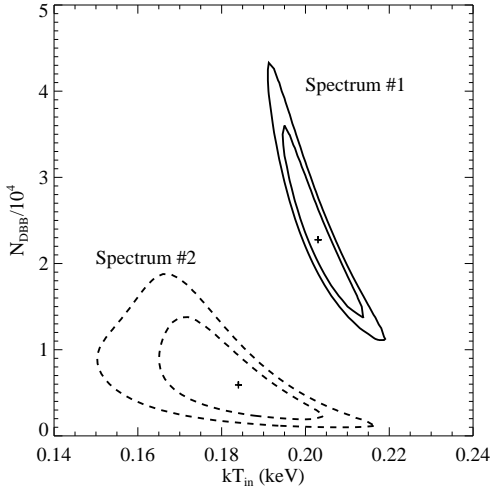


FIG. 4.— Confidence contours for the thermal (disk-blackbody) components for Spectra #1 (solid contours) and #2 (dashed contours). In each case, the inner-most contour encircles the 68% confidence ($\Delta\chi^2 = 2.30$) error region for the two parameters and the outer-most contour corresponds to 90% confidence ($\Delta\chi^2 = 4.61$).

energy range suggest that there is indeed a reflection component. Thus, we re-fitted the spectra with a model consisting of a disk-blackbody, an iron emission line, and a `pexriv` reflection component (Magdziarz & Zdziarski 1995), which includes both direct emission from a power-law as well as emission reflected off an accretion disk with neutral or partially ionized material. While the `pexriv` model includes the ionization effects, which are likely important for the hot accretion disks around X-ray binaries, it does not include relativistic smearing. Thus, in our model, we convolved the `pexriv` model with the `laor` model shape using the XSPEC convolution model `kdblur`. We set up the XSPEC model so that `kdblur` convolves the sum of a narrow iron line and the `pexriv` model. The `kdblur` parameters include R_{in} (the inner radius of the disk), R_{out} (the outer radius of the disk), i (the binary inclination), and q (the power-law index for the radial emissivity profile).

The results of these fits are given in Table 3, and the fit-

ted spectra are shown in Figures 5 and 6. The power-law and disk-blackbody parameters have similar values to those that we found with the basic models (Table 2), and the quality of the fits is better than we obtained with the basic models. For both spectra, the presence of the `pexriv` reflection component is required at high confidence as indicated by the fact that the reflection covering fraction ($\Omega/2\pi$) is significantly different from zero. The exact value of $\Omega/2\pi$ depends strongly on the binary inclination, which is not known for GX 339–4. Previous fits to higher quality X-ray spectra have given a value of $i = 20^{+5}_{-15}$ degrees (Miller et al. 2006), and we adopt a value of 20° to facilitate comparisons to the previous work. With this inclination, we obtain values of $\Omega/2\pi = 0.22^{+0.06}_{-0.05}$ and $0.24^{+0.11}_{-0.08}$ for Spectra #1 and #2, respectively. The `pexriv` ionization parameter, ξ , is not very well-constrained, but it is significantly greater than zero for both spectra, indicating a disk that is at least partially ionized.

While the reflection component is statistically significant in both Spectra #1 and #2, an additional iron line in the 6.4–7.1 keV range (see E_{line} in Table 3) is required for Spectrum #1 but is required at only slightly more than 90% confidence for Spectrum #2 as shown by the values of the emission line normalization (N_{line}) given in Table 3. This is not due to the lack of iron features in Spectrum #2 but because, with the relativistic broadening, the reflection component contains a bump related to the iron absorption edge that can mimic a broad iron emission line (see Figures 5 and 6). However, even though the emission line is not clearly detected in Spectrum #2, the parameters that account for the relativistic smearing are still well-constrained for both spectra because both the line and the reflection (`pexriv`) components are smeared.

While there are four relativistic smearing parameters, only two of the parameters are left as free parameters in our fits. As mentioned above, we fixed the binary inclination to 20° , and we fixed the outer disk radius to $R_{\text{out}} = 400R_g (= GM/c^2)$, where G and c are constants and M is the black hole mass). One of the free parameters is the inner disk radius, and we find that $R_{\text{in}} = 3.6^{+1.4}_{-1.0}R_g$ and $2.9^{+2.1}_{-0.7}R_g$ for Spectra #1 and #2, respectively, implying that the reflecting material is very close to the black hole. The other free parameter is the power-law index for the radial emissivity profile, and we obtain values consistent with $q = 3$ for both spectra.

5. DISCUSSION

5.1. Constraints from the Reflection Model

Our results on the iron line and reflection component of GX 339–4 join a relatively small number of observations where reflection models that account for the relativistic effects near black holes have been fitted to broadband X-ray spectra of black holes in the hard state. Our findings are most directly comparable to the results of Miller et al. (2006) where both the GX 339–4 and Cygnus X-1 showed evidence for a broad iron $K\alpha$ emission line and a smeared reflection component while they were in the hard state. Table 3 compares the parameters for GX 339–4 from the fits to the 2004 *XMM-Newton/RXTE* spectrum reported in Miller et al. (2006) to the parameters we obtain by fitting the same model to our *Swift/RXTE* spectra. Independent of assumptions about the distance to the source, Spectra #1 and #2 were taken when the GX 339–4 luminosity (1–100 keV, unabsorbed) was, respectively, 2.4 and 7.0 times lower than the 2004 spectrum. Adopting a source distance of 8 kpc (Hynes et al. 2004) and a black hole mass of $5.8M_\odot$ (Hynes et al. 2003), which are

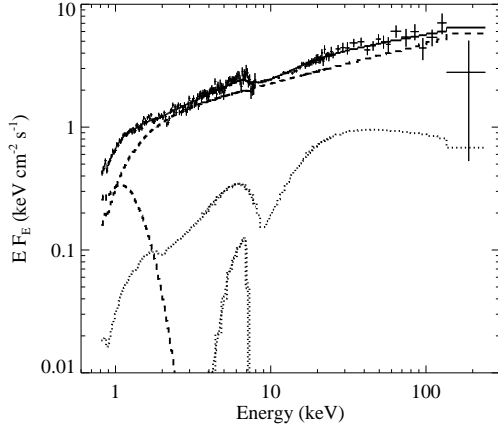


FIG. 5.— Spectrum #1 fitted with the model detailed in Table 3 and plotted in flux units. The various model components are shown and include a thermal disk-blackbody component, a power-law, a reflection component, and an iron emission line (the last two include relativistic effects).

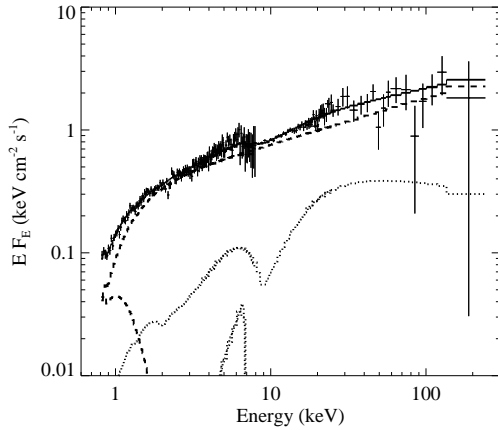


FIG. 6.— Spectrum #2 fitted with the model detailed in Table 3 and plotted in flux units. The various model components are shown and include a thermal disk-blackbody component, a power-law, a reflection component, and an iron emission line (the last two include relativistic effects).

the same values used by Miller et al. (2006), we estimate that the Eddington-scaled luminosities during our observations are $L/L_{\text{Edd}} = 0.023$ and 0.008 .

The two most significant reflection parameters for answering the question of the accretion geometry for GX 339–4 in the hard state are the covering fraction $\Omega/2\pi$ and the inner radius of the optically thick disk ($r_{\text{in}} = R_{\text{in}}/R_{\text{g}}$). The covering fraction of ~ 0.23 that we obtain (assuming $i = 20^\circ$) is consistent with the value of 0.22 ± 0.06 obtained by Miller et al. (2006), and this may indicate little change in the system geometry even though we are observing at a lower flux. However, these values of $\Omega/2\pi$ are much less than the values of unity or even larger that have been seen for GX 339–4 as well as other black hole systems in the SPL state (Zdziarski et al. 2003; Miller et al. 2004). Although we are including relativistic effects that were not included in earlier work by Zdziarski et al. (2003), our covering fraction and power-law index (Γ) values are very similar to the values Zdziarski et al. (2003) used to demonstrate a systematic drop in the covering fraction as the source hardens. Thus, these results are consistent with a significant change in geometry between the SPL

and the hard state, but not in the hard state between 0.056 and $0.008 L_{\text{Edd}}$. In addition, we note that geometry is not necessarily the only change that occurs between the SPL and the hard state.

The inner disk radii implied by the reflection model parameters also suggest little or no change in r_{in} down to $0.008 L_{\text{Edd}}$. While Miller et al. (2006) obtain $r_{\text{in}} = 4.0 \pm 0.5$, our reflection fits indicate *maximum* (90% confidence) r_{in} values of 5.0 for for Spectra #1 and #2, and the spectra are consistent with little change from $r_{\text{in}} \sim 4$ over the 0.008 – $0.056 L_{\text{Edd}}$ luminosity range. However, for Spectrum #2, since the iron line is not required at high statistical confidence, we re-fitted the spectrum without the emission line, allowing only the blurred reflection component to constrain r_{in} . In this case, we obtain $r_{\text{in}} = 4.1^{+5.9}_{-1.4}$ so that we should not rule out the possibility that the inner disk radius increases to $\sim 10 R_{\text{g}}$ at the lowest luminosity that we are sampling.

Of course, these radius constraints are only valid if the blurring that is clearly present is caused by the Doppler boosting due to the motions of the material around the black hole and the gravitational redshift, and it is worthwhile to consider whether other physical effects could cause similar blurring. Probably the best developed competing model attributes the reflection component to Compton downscattering of the source’s X-ray emission in a large-scale and powerful wind (Titarchuk & Shrader 2005). The model requires hard X-ray emission with a power-law photon index of $\Gamma < 2$, and the model has been shown to be able to reproduce the shape of the ~ 20 – 200 keV hard state spectra from GX 339–4 (Titarchuk & Shrader 2005). More recently, it was shown that this Comptonization model can produce blurred and redshifted iron lines due to fluorescence of the wind material (Laurent & Titarchuk 2007). Although this full model is not currently available for fitting our GX 339–4 spectra, in the future, it would be interesting to see if it can explain all the spectral features we observe.

5.2. The Thermal Component in the Hard State

Further evidence for an optically thick disk in the hard state that is not highly truncated comes from the presence of a thermal component that has now been seen in the hard state spectra of several black hole systems. In our case, Spectrum #1 has a significant thermal component while the thermal component may be present in Spectrum #2, but it is not required at very high significance. Thus, we focus on comparing our Spectrum #1 parameters to the disk-blackbody parameters found by Miller et al. (2006). As shown in Table 3, the inner disk temperature of 0.193 ± 0.012 keV for Spectrum #1 is significantly lower than the value of $kT_{\text{in}} = 0.39 \pm 0.04$ keV measured when the 3–100 keV flux of the source was 2.4 times brighter. While a drop in temperature does not necessarily signal a change in accretion geometry, the disk-blackbody normalization is related to the disk inner radius according to $N_{\text{DBB}} \propto R_{\text{in}}^2$, so the fact that N_{DBB} is significantly larger for Spectrum #1 (see Table 3) could indicate an increase in R_{in} .

To further investigate the difference between the values of N_{DBB} in the two spectra, we note that for these low temperatures, the disk component is strongly impacted by interstellar absorption, and the value of N_{H} that we obtain is somewhat higher than the value derived by Miller et al. (2006). Thus, we refitted Spectrum #1 after fixing the column density to the Miller et al. (2006) value. We obtain only a slightly higher temperature of $kT_{\text{in}} = 0.220 \pm 0.013$ keV and $N_{\text{DBB}} =$

6100^{+2800}_{-1500} . Thus, N_{DBB} is still nearly an order of magnitude higher for Spectrum #1 compared to the value of ~ 700 obtained by Miller et al. (2006). Another (not independent) way to examine the question of whether R_{in} changes is that the disk-blackbody flux (F_{disk}) should be proportional to kT_{in}^4 for constant R_{in} (Mitsuda et al. 1984). Based on the parameters with N_{H} fixed, the bolometric disk-blackbody flux for Spectrum #1 is $3.2 \times 10^{-10} \text{ ergs cm}^{-2} \text{ s}^{-1}$, while the flux from the Miller et al. (2006) parameters is $3.4 \times 10^{-10} \text{ ergs cm}^{-2} \text{ s}^{-1}$. While the fact that these fluxes are nearly the same despite a drop in kT_{in} from 0.39 keV to 0.22 keV could be explained by a change in R_{in} , other physical effects could also be important such as possible changes in the “color correction factor” (Shimura & Takahara 1995) or changes in the temperature profile in the disk. It is also worth noting that the observations were made with different soft X-ray instruments (*XMM-Newton* vs. *Swift*) and differences in calibration could be important. However, despite these other possibilities, if the correct explanation is a change in the inner radius, R_{in} would need to change by a factor of ~ 3 .

Our results for the evolution of the disk-blackbody parameters appear to be in contrast to results obtained recently by Rykoff et al. (2007) for another accreting black hole (XTE J1817–330) in the hard state. Using ~ 20 *Swift* observations covering inner disk temperatures from 0.2 to 0.8 keV, Rykoff et al. (2007) found a relationship close to $F_{\text{disk}} \propto kT_{\text{in}}^4$ (they actually found an index of 3.3 ± 0.1 or 4.3 ± 0.1 depending on the model they used for the non-thermal component). Although XTE J1817–330 does show some deviations from the trend for individual data points (see Figure 3 from Rykoff et al. 2007), none of the deviations from the $F_{\text{disk}} \propto kT_{\text{in}}^4$ trend are as large as we see for GX 339–4, suggesting that we may be seeing a different evolution for GX 339–4.

5.3. Implications for the Hard State Geometry

Our spectra of GX 339–4 provide evidence for an optically thick accretion disk in the hard state. At $L/L_{\text{Edd}} = 0.023$, the evidence comes from both blurred reflection and iron line features as well as a significant thermal component. At $L/L_{\text{Edd}} = 0.008$, the evidence primarily comes from the blurred reflection component. The most constraining measurement of r_{in} comes from the reflection component, and these measurements require $r_{\text{in}} < 5$ at $0.023 L_{\text{Edd}}$ and $r_{\text{in}} < 10$ at $0.008 L_{\text{Edd}}$. If the value of $r_{\text{in}} = 2\text{--}3$ measured in the SPL state represents the location of the ISCO, then our hard state measurements imply a change of no more than a factor of 2.5 and 5 (for the two luminosities, respectively) greater than the radius of the ISCO (although see caveats discussed above).

Recent theoretical work suggests a possible geometry that may be consistent with these observations. It is found that two physical processes can be important to causing material to condense out of an ADAF, leaving an inner optically thick disk. First, as an ADAF is forming, the material close to the ADAF/disk boundary will be significantly cooled via conductive cooling, and will cause ADAF material to recondense back into the disk (Meyer, Liu & Meyer-Hofmeister 2007). Secondly, the soft photons from the optically thick disk can Compton-cool the ADAF, which also leads to condensation (Liu et al. 2007). For a relatively large range of mass accretion rates and viscosity parameters, these effects lead to inner and outer optically thick disks with an ADAF filling the gap in between. As discussed in Liu et al. (2007), such a model

would apply for the brighter portion of the hard state and could explain the small inner radii inferred from reflection fits in the hard state and the $\sim 0.2\text{--}0.3$ keV thermal components. This geometry is also at least qualitatively consistent with the observed $\Omega/2\pi$ values.

Although such condensation can occur for relatively bright portions of the hard state, the calculations of Liu et al. (2007) still indicate that below $L/L_{\text{Edd}} \sim 0.001$, the inner disk will evaporate, leaving only ADAF inside some truncation radius. Thus, it is notable that our observations of GX 339–4 as well as most, if not all, of the cases where small inner disk radii have been inferred for the hard state via reflection modeling or the presence of soft components have occurred above this level (Miller, Homan & Miniutti 2006; Rykoff et al. 2007). At lower luminosity, there have been observations that do not necessarily require soft components in the X-ray band. For example, for the black hole system XTE J1118+480, McClintock et al. (2001) find evidence for a soft component at the very low temperature of ~ 24 eV when the system was near $0.001 L_{\text{Edd}}$ (assuming a distance of 1.8 kpc and a black hole mass of $7 M_{\odot}$). In addition, Tomsick, Kalemci & Kaaret (2004) observed XTE J1650–500 at levels of $10^{-4} L_{\text{Edd}}$ (assuming a distance of 4 kpc and a black hole mass of $10 M_{\odot}$), and did not detect a soft component or iron features. Finally, very high quality spectra have been obtained for several systems in quiescence $L/L_{\text{Edd}} \sim 10^{-6}$ or lower without evidence for a thermal component or iron features (e.g., Bradley et al. 2007; Corbel, Tomsick & Kaaret 2006).

5.4. Implications for the Compact Jet

The possibility of an inner optically thick disk in the hard state has very interesting implications for the production of compact jets in the hard state. For GX 339–4, we detect the compact jet in the radio band contemporaneously with the times that we obtained Spectra #1 and #2, and Miller et al. (2006) also report the presence of a compact jet during their hard state observation. Cygnus X-1 provides another example of a bright hard state black hole with a compact jet. These examples imply that a compact jet can be produced when the inner optically thick disk is present. Furthermore, it is notable that fitting multi-wavelength spectral energy distributions from radio-to-X-ray observations of GX 339–4, Cygnus X-1, and another black hole system, GRO J1655–40, with a compact jet model give values of $3.5\text{--}10 R_{\text{g}}$ for the radius of the jet at its base (Markoff, Nowak & Wilms 2005; Migliari et al. 2007). These small radii are consistent with the jet being launched at or within the inner edge of the disk, and may imply that the production of the compact jet is closely linked to the inner disk.

However, at the same time, radio observations show that compact jets can also be produced at very low luminosities by quiescent black holes (Gallo, Fender & Hynes 2005; Gallo et al. 2006). This brings the role of the inner disk in jet production into question since it is unclear whether the inner disk persists to these low luminosities. As discussed above, the conductive and Compton cooling mechanisms considered by Liu et al. (2007) indicate that the disk should evaporate below $0.001 L_{\text{Edd}}$. However, it may still be worth considering whether other cooling mechanisms can maintain the inner disk to lower levels. For example, Meier (2005) has explored the possibility of Magnetically Dominated Accretion Flows (MDAFs), and there are indications for an inner disk region in the hard state where magnetic cooling is important. Clearly,

more theoretical studies as well as observations at these very low luminosities are important for a full understanding the full set of conditions that are required for compact jet production.

TABLE 1
OBSERVATIONS OF GX 339–4

Satellite	Observation ID (ObsID)	Date in 2007	Start Time (UT hour)	Stop Time (UT hour)	Exposure ^a (s)
Spectrum #1					
<i>Swift</i>	00030943001	May 25	17.10	23.80	6150
<i>RXTE</i>	92704-04-02-00	May 25	17.99	20.13	4976
<i>RXTE</i>	92704-04-02-02	May 25	21.14	21.69	1808
Spectrum #2					
<i>Swift</i>	00030943002	June 10	16.70	21.70	4685
<i>Swift</i>	00030943003	June 12	1.29	21.98	5509
<i>Swift</i>	00030943004	June 14	1.01	22.38	3204
<i>RXTE</i>	92704-03-28-00	June 10	4.43	5.63	2320
<i>RXTE</i>	92704-03-29-00	June 11	8.44	9.51	3392
<i>RXTE</i>	94704-03-29-01	June 12	3.27	3.64	1056
<i>RXTE</i>	94704-03-30-00	June 13	6.08	6.64	1952
<i>RXTE</i>	94704-03-31-00	June 14	15.29	16.28	2112

^aThis is the exposure time on the target (GX 339–4) obtained by the XRT instrument (for *Swift*) or the PCA instrument (for *RXTE*).

JAT would like to thank Sergio Campana for information about the *Swift*/XRT calibration. JAT thanks Tomaso Belloni, Jon Miller, and Jeroen Homan for useful discussions. We would like to thank Neil Gehrels for approving the second set of *Swift* observations. We appreciate comments from the anonymous referee that helped to improve this paper. JAT

acknowledges partial support from NASA RXTE Guest Observer grants NNG06GA81G and NNX06AG83G. EK is supported by TÜBİTAK Career Development Award 106T570 and also by a Turkish National Academy of Sciences Young and Successful Scientist Award.

REFERENCES

- Balucinska-Church, M., & McCammon, D., 1992, *ApJ*, 400, 699
Bradley, C. K., Hynes, R. I., Kong, A. K. H., Haswell, C. A., Casares, J., & Gallo, E., 2007, *ApJ*, 667, 427
Bradt, H. V., Rothschild, R. E., & Swank, J. H., 1993, *A&AS*, 97, 355
Burrows, D. N., et al., 2005, *Space Science Reviews*, 120, 165
Buxton, M., & Bailyn, C., 2007, *The Astronomer's Telegram*, 1109
Corbel, S., Tomsick, J. A., & Kaaret, P., 2006, *ApJ*, 636, 971
Dove, J. B., Wilms, J., Maisack, M., & Begelman, M. C., 1997, *ApJ*, 487, 759
Ebisawa, K., et al., 1994, *PASJ*, 46, 375
Ebisawa, K., Ueda, Y., Inoue, H., Tanaka, Y., & White, N. E., 1996, *ApJ*, 467, 419
Esin, A. A., McClintock, J. E., & Narayan, R., 1997, *ApJ*, 489, 865
Fender, R. P., 2001, *MNRAS*, 322, 31
Fender, R. P., Hjellming, R. M., Tilanus, R. P. J., Pooley, G. G., Deane, J. R., Ogle, R. N., & Spencer, R. E., 2001, *MNRAS*, 322, L23
Gallo, E., Fender, R. P., & Hynes, R. I., 2005, *MNRAS*, 356, 1017
Gallo, E., Fender, R. P., Miller-Jones, J. C. A., Merloni, A., Jonker, P. G., Heinz, S., Maccarone, T. J., & van der Klis, M., 2006, *MNRAS*, 370, 1351
Gehrels, N., et al., 2004, *ApJ*, 611, 1005
Homan, J., & Belloni, T., 2005, *Ap&SS*, 300, 107
Hynes, R. I., Steeghs, D., Casares, J., Charles, P. A., & O'Brien, K., 2003, *ApJ*, 583, L95
Hynes, R. I., Steeghs, D., Casares, J., Charles, P. A., & O'Brien, K., 2004, *ApJ*, 609, 317
Jahoda, K., Markwardt, C. B., Radeva, Y., Rots, A. H., Stark, M. J., Swank, J. H., Strohmayer, T. E., & Zhang, W., 2006, *ApJS*, 163, 401
Kalemci, E., et al., 2007, *The Astronomer's Telegram*, 1074
Kalemci, E., Tomsick, J. A., Rothschild, R. E., Pottschmidt, K., & Kaaret, P., 2004, *ApJ*, 603, 231
Laor, A., 1991, *ApJ*, 376, 90
Laurent, P., & Titarchuk, L., 2007, *ApJ*, 656, 1056
Liu, B. F., Taam, R. E., Meyer-Hofmeister, E., & Meyer, F., 2007, *ApJ*, 671, 695
Maccarone, T. J., 2003, *A&A*, 409, 697
Magdziarz, P., & Zdziarski, A. A., 1995, *MNRAS*, 273, 837
Markoff, S., Nowak, M. A., & Wilms, J., 2005, *ApJ*, 635, 1203
McClintock, J. E., et al., 2001, *ApJ*, 555, 477
McClintock, J. E., Narayan, R., Garcia, M. R., Orosz, J. A., Remillard, R. A., & Murray, S. S., 2003, *ApJ*, 593, 435
McClintock, J. E., & Remillard, R. A., 2006, *Black hole binaries, Compact stellar X-ray sources*. Edited by Walter Lewin & Michiel van der Klis: Cambridge University Press, 157–213
Meier, D. L., 2005, *Ap&SS*, 300, 55
Meyer, F., Liu, B. F., & Meyer-Hofmeister, E., 2000, *A&A*, 361, 175
Meyer, F., Liu, B. F., & Meyer-Hofmeister, E., 2007, *A&A*, 463, 1
Migliari, S., et al., 2007, *ApJ*, 670, 610
Miller, J. M., et al., 2004, *ApJ*, 606, L131
Miller, J. M., et al., 2002, *ApJ*, 570, L69
Miller, J. M., Homan, J., & Miniutti, G., 2006, *ApJ*, 652, L113
Miller, J. M., Homan, J., Steeghs, D., Rupen, M., Hunstead, R. W., Wijnands, R., Charles, P. A., & Fabian, A. C., 2006, *ApJ*, 653, 525
Miller, J. M., Kuulkers, E., Caballero-Garcia, M. D., & Diaz Trigo, M., 2007, *The Astronomer's Telegram*, 980
Mitsuda, K., et al., 1984, *PASJ*, 36, 741
Narayan, R., McClintock, J. E., & Yi, I., 1996, *ApJ*, 457, 821
Osborne, J. P., et al., 2005, in *UV, X-Ray, and Gamma-Ray Space Instrumentation for Astronomy XIV*. Edited by Siegmund, Oswald H. W. *Proceedings of the SPIE*, Volume 5898, pp. 352–359 (2005), ed. O. H. W. Siegmund, Vol. 5898, 352
Poutanen, J., Krolik, J. H., & Ryde, F., 1997, *MNRAS*, 292, L21
Predehl, P., & Schmitt, J. H. M. M., 1995, *A&A*, 293, 889
Remillard, R. A., Sobczak, G. J., Munro, M. P., & McClintock, J. E., 2002, *ApJ*, 564, 962
Revnivtsev, M., Gilfanov, M., & Churazov, E., 2001, *A&A*, 380, 520
Reynolds, C. S., & Nowak, M. A., 2003, *Phys.Rep.*, 377, 389
Rothschild, R. E., et al., 1998, *ApJ*, 496, 538
Rykoff, E. S., Miller, J. M., Steeghs, D., & Torres, M. A. P., 2007, *ApJ*, 666, 1129
Shakura, N. I., & Sunyaev, R. A., 1973, *A&A*, 24, 337
Shimura, T., & Takahara, F., 1995, *ApJ*, 445, 780
Thorne, K. S., 1974, *ApJ*, 191, 507
Titarchuk, L., & Shrader, C., 2005, *ApJ*, 623, 362
Tomsick, J. A., & Kaaret, P., 2000, *ApJ*, 537, 448
Tomsick, J. A., Kalemci, E., & Kaaret, P., 2004, *ApJ*, 601, 439
Wilms, J., Allen, A., & McCray, R., 2000, *ApJ*, 542, 914
Zdziarski, A. A., Lubinski, P., Gilfanov, M., & Revnivtsev, M., 2003, *MNRAS*, 342, 355
Zdziarski, A. A., Lubinski, P., & Smith, D. A., 1999, *MNRAS*, 303, L11
Zdziarski, A. A., Poutanen, J., Mikolajewska, J., Gierlinski, M., Ebisawa, K., & Johnson, W. N., 1998, *MNRAS*, 301, 435

TABLE 2
GX 339–4 SPECTRAL FITS WITH BASIC MODELS

Model ^a	N_{H}^b (10^{21} cm^{-2})	Γ	N_{PL}^c	kT_{in} (keV)	N_{DBB}	χ^2/ν
Spectrum #1						
PL	3.1 ± 0.1	1.66 ± 0.01	0.113 ± 0.002	—	—	651.8/213
PL+DBB	8.5 ± 0.7	1.69 ± 0.01	0.125 ± 0.003	0.178 ± 0.007	$76,000^{+39,000}_{-26,000}$	532.0/211
SM \times PL	2.6 ± 0.1	1.58 ± 0.01	0.104 ± 0.002	—	—	444.7/211
SM \times (PL+DBB)	7.2 ± 0.7	1.59 ± 0.02	0.109 ± 0.003	$0.203^{+0.012}_{-0.010}$	$23,000^{+15,000}_{-10,000}$	338.3/209
Spectrum #2						
PL	4.9 ± 0.2	1.61 ± 0.02	0.0329 ± 0.0008	—	—	321.6/213
PL+DBB	9.0 ± 1.1	1.64 ± 0.02	0.0367 ± 0.0013	0.157 ± 0.011	$35,000^{+30,000}_{-18,000}$	280.1/211
SM \times PL	4.2 ± 0.2	1.50 ± 0.02	0.0294 ± 0.0008	—	—	210.6/211
SM \times (PL+DBB)	7.0 ± 1.4	1.52 ± 0.03	0.0315 ± 0.0015	$0.184^{+0.023}_{-0.022}$	$5,900^{+8,700}_{-4,300}$	200.2/209

^aPL is a power-law model. DBB is the Mitsuda et al. (1984) disk-blackbody model. SM is the smeared iron edge model from Ebisawa et al. (1994). For these fits, we fixed the width of the smeared iron edge to 10 keV.

^bErrors on all parameter values are 90% confidence ($\Delta\chi^2 = 2.7$).

^cUnits are photons $\text{cm}^{-2} \text{ s}^{-1} \text{ keV}^{-1}$ at 1 keV.

TABLE 3
GX 339–4 SPECTRAL FITS WITH REFLECTION

Parameter ^a	Spectrum #1	Spectrum #2	2004 Spectrum ^b
N_{H} (10^{21} cm^{-2})	$7.1^{+0.9}_{-0.8}$	$7.3^{+1.5}_{-1.3}$	3.7 ± 0.4
Γ	$1.68^{+0.03}_{-0.02}$	$1.63^{+0.04}_{-0.03}$	1.41 ± 0.03
N_{PL}^c	$0.118^{+0.008}_{-0.006}$	$0.035^{+0.004}_{-0.003}$	0.32 ± 0.03
kT_{in} (keV)	0.193 ± 0.012	$0.161^{+0.017}_{-0.031}$	0.39 ± 0.04
N_{DBB}	$29,000^{+27,000}_{-14,000}$	$14,000^{+35,000}_{-9,000}$	700 ± 200
i (degrees)	20.0	20.0	20^{+5}_{-15}
$\Omega/2\pi^d$ (pexriv)	$0.22^{+0.06}_{-0.05}$	$0.24^{+0.11}_{-0.08}$	0.22 ± 0.06
ξ^e (ergs $\text{cm}^{-1} \text{ s}^{-1}$) (pexriv)	$10,000^{+6,000}_{-5,000}$	$7,000^{+8,000}_{-4,000}$	1,000
E_{line} (keV)	$6.9^{+0.2}_{-0.5}$	$6.7^{+0.4}_{-0.3}$	6.8 ± 0.1
N_{line} (photons $\text{cm}^{-2} \text{ s}^{-1}$)	$(7.4 \pm 4.4) \times 10^{-4}$	$(2.4^{+2.6}_{-2.1}) \times 10^{-4}$	$(3.5 \pm 0.3) \times 10^{-3}$
$R_{\mathrm{in}}/R_{\mathrm{g}}$ (kdblur)	$3.6^{+1.4}_{-1.0}$	$2.9^{+2.1}_{-0.7}$	4.0 ± 0.5
q^f (kdblur)	$3.2^{+0.5}_{-0.6}$	3.1 ± 0.4	3.0
χ^2/ν	324.7/205	191.3/205	2120.5/1160
Absorbed Flux (ergs $\text{cm}^{-2} \text{ s}^{-1}$) ^g	2.1×10^{-9}	7.4×10^{-10}	5.4×10^{-9}
Unabs. Flux (ergs $\text{cm}^{-2} \text{ s}^{-1}$) ^h	2.2×10^{-9}	7.7×10^{-10}	5.5×10^{-9}
Luminosity (ergs s^{-1}) ⁱ	1.7×10^{37}	5.9×10^{36}	4.2×10^{37}
Luminosity (L_{Edd}) ^j	0.023	0.008	0.056
Iron Line Equivalent Width (eV)	140 ± 90	140^{+150}_{-120}	~ 160

^aErrors on all parameter values are 90% confidence ($\Delta\chi^2 = 2.7$).

^bThese are the parameters obtained by Miller et al. (2006) for the 2004 *XMM-Newton* and *RXTE* observations of GX 339–4.

^cUnits are photons $\text{cm}^{-2} \text{ s}^{-1} \text{ keV}^{-1}$ at 1 keV.

^dReflection covering factor.

^eIonization parameter.

^fThe power-law index for the radial emissivity profile.

^gAbsorbed flux in the 1–100 keV band.

^hUnabsorbed flux in the 1–100 keV band.

ⁱ1–100 keV luminosity assuming a distance of 8 kpc.

^j1–100 keV luminosity in Eddington units assuming a distance of 8 kpc and a black hole mass of $5.8 M_{\odot}$.